Optical and electrical properties of indium sulfide thin film prepared by magnetron sputtering

YINGZHUO SHENG[a,b], JUNQIANG QIAO[a,*], XUELIANG LV[b], ZHENXING ZHANG[b,*]
[a]*Key Laboratory of Photovoltaic, Gansu Province, Gansu Natural Energy Research Institute, Gansu Academy of Sciences, Lanzhou 730000, China*
[b]*Key Laboratory of Special Function Materials and Structure Design of the Ministry of Education, Key Laboratory for Magnetism and Magnetic Materials of the Ministry of Education, School of Physical Science and Technology, Lanzhou University, Lanzhou 730000, China*

Indium sulfide thin films were prepared by radio-frequency sputtering. The as-prepared films are amorphous independent of the sputtering power and growth times. The subsequent annealing effect on the crystallinity, optical properties, and photoelectric conversion properties was investigated. The annealed films are β-In_2S_3, and their indirect optical band gaps are from 2.04 to 2.20 eV as the annealing temperature increases from 300 ℃ to 500 ℃. The photovoltaic conversion of the In_2S_3/Si heterostructure is also demonstrated.

(Received January 11, 2021; accepted November 24, 2021)

Keywords: Indium sulfide, Sputtering, Annealing, Photovoltaics, Thin film

1. Introduction

Indium sulfide (In_2S_3) is a typical n-type III-VI semiconductor material [1, 2]. It has three different crystal structures: α (cubic), β (spinel), and γ phases (trigonal layered structure) [3]. Among them, β-In_2S_3 with a bandgap of 2.00-2.30 eV has received considerable attention due to its unique chemical and optical properties and facile preparation methods[4]. It has been widely used as a buffer layer or intermediate band material in solar cells[5, 6, 7], host in photocatalyts[8, 9, 10], a light-sensitive material for ultrasensitive photodector[4, 11], and many other applications[12, 13, 14]. A variety of approaches have been explored to prepare high-quality In_2S_3 thin films, including thermal evaporation[15], chemical vapor deposition[4], electrodeposition[16], atomic layer deposition[17], spray pyrolysis[18], and sputtering[19, 20, 21, 22].

Sputtering is an economical and facile synthesis method and would be potentially suitable for the mass applications of In_2S_3 thin films [23]. Yanxin Ji et al. reported the radio-frequency sputtered In_2S_3 layers are single tetragonal phase with (103) preferred orientation with a direct bandgap of 2.44~2.66 eV and an indirect bandgap of 1.82~2.06 eV dependent on the thickness of the films[21]. Sreejith Karthikeyan et al. reported that the pulsed direct current magnetron sputtering prepared In_2S_3 is a single β phase with a direct bandgap of 2. 77 eV[20]. Dong Hyun Hwang et al. reported the radio-frequency sputtered In_2S_3 films are polycrystalline β structure. The grain size increases from 7 nm to 13 nm, and the direct optical band gap of the film decreases from 2.88 eV to 2.43 eV as the sputtering increases from 60 W to 120 W[22]. However, the electrical properties of sputtered In_2S_3 films on silicon substrates are rarely investigated, especially the photoelectric conversion properties.

Herein, indium sulfide thin films were prepared by sputtering. The subsequent annealing effect on the crystallinity, optical properties, and photoelectric conversion properties were also investigated. The annealed films are β-In_2S_3, and their indirect optical band gaps are from 2.04 to 2.20 eV as the annealing temperature increases from 300 °C to 500 °C. The photovoltaic conversion of the In_2S_3/Si heterostructure is also demonstrated

2. Experimental

Indium sulfide thin films were grown on p-type Si (100) and glass substrates by radio frequency magnetron sputtering in nitrogen gas. The In_2S_3 target with a purity of 99.9%, a diameter of 3 inch, and a thickness of 5 mm was purchased from Beijing Guoxin Youyuan Technology Co., Ltd, China. Before the sputtering, a background pressure of $1.0*10^{-3}$ Pa was obtained. The substrate was no intentionally heated during the sputtering. The sputtering pressure was kept at 1 Pa, and the deposition time was 1 h. The subsequent annealing was conducted in the tube furnace from 573 K to 773 K in Ar gas for 3h. The Au contacts for electrical characterization were constructed by sputtering of Au foil through a metal shadow mask with 1 mm diameter of the pores and 5 mm spacing between

circular dots in a small ion sputter (MSBC-12).

The deposited films' structure characteristics were determined by GIXRD using a Philips X'Pert diffractometer with Cu Kα1 radiation (λ=1.54056 Å). Raman spectroscopy was performed on a Jobin-Yvon LabRam HR80 spectrometer with a 532 nm line of 50 mW diode-pumped solid-state laser at room temperature. Ultraviolet-Visible (UV–Vis) spectrum was measured by spectrophotometer (PGENERAL TU1901). The electrical properties were evaluated by a semiconductor characterization system (KEITHLEY 4200-SCS). The photocurrent density-voltage (J-V) curves were measured under a solar simulator (Zolix, China) with an intensity of 100 mW cm^{-2} (AM 1.5G).

3. Results and discussion

The effects of sputtering power and growth time on the properties of the films were systematically studied. It can be seen from Fig. 1a that the films prepared at the power from 60 W to 200 W with the growth time from 10 min to 40 min are all amorphous. As shown in Fig. 1b, the films prepared only at low powers of 60 W and 100 W with a growth time of 10 min present a very weak peak around 301 cm^{-1}, which can be attributed to the vibration of InS_4 tetrahedra [24]. Larger power or growth time will weaken this characteristic Raman peak, verifying the amorphous nature of the films from XRD results. UV-Vis spectra show that the films absorb UV and visible light to some extent (Fig. 1c). With the increase of growth time and power, the absorption edge shifts to the long-wavelength direction, indicating a smaller bandgap of the films. Meanwhile, transmission spectra show apparent peaks and valleys due to interference [25].

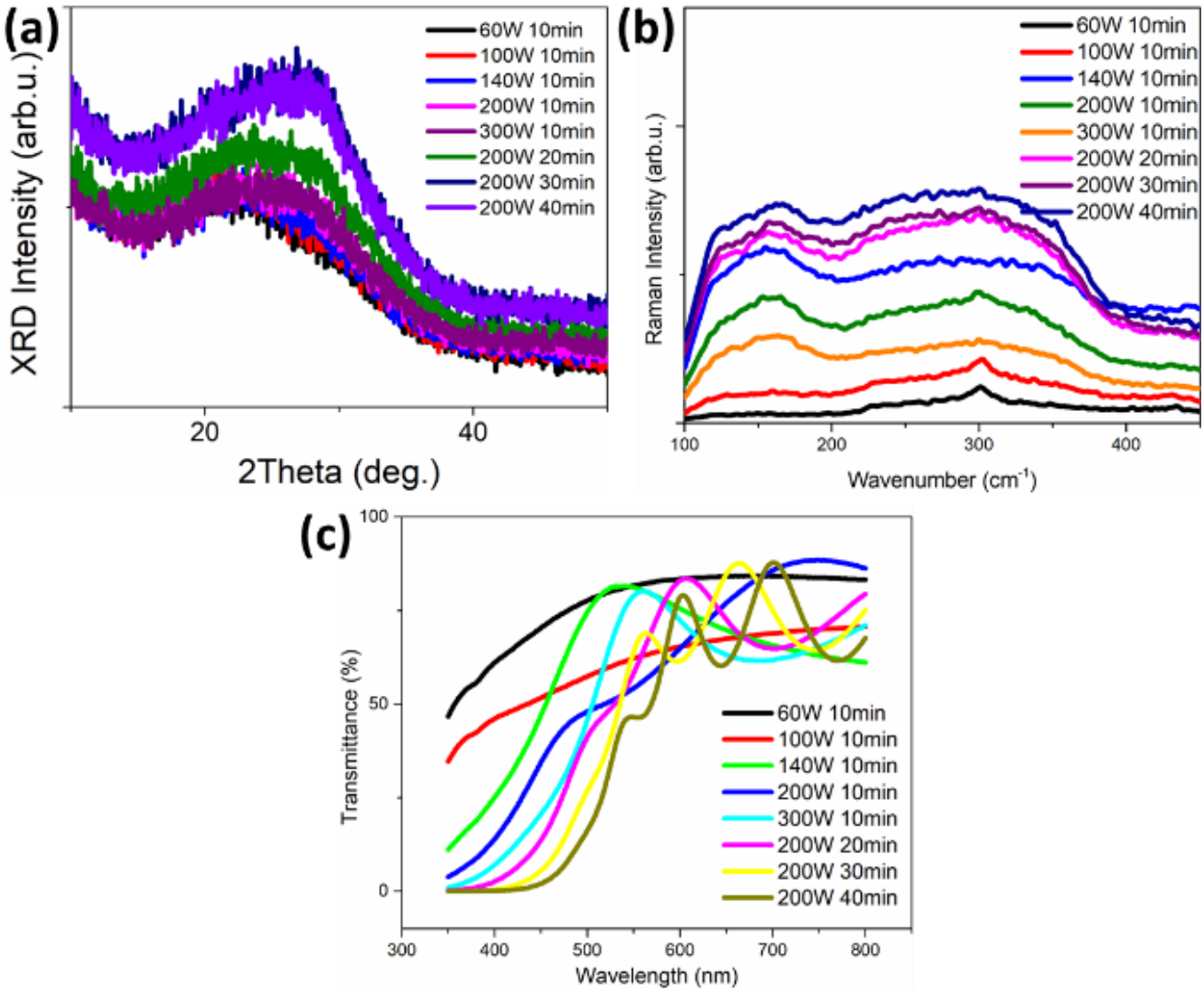

Fig. 1. (a) XRD pattern, (b) Raman spectra and (c) UV-Vis spectra of the films prepared by sputtering at different powers and growth times (color online)

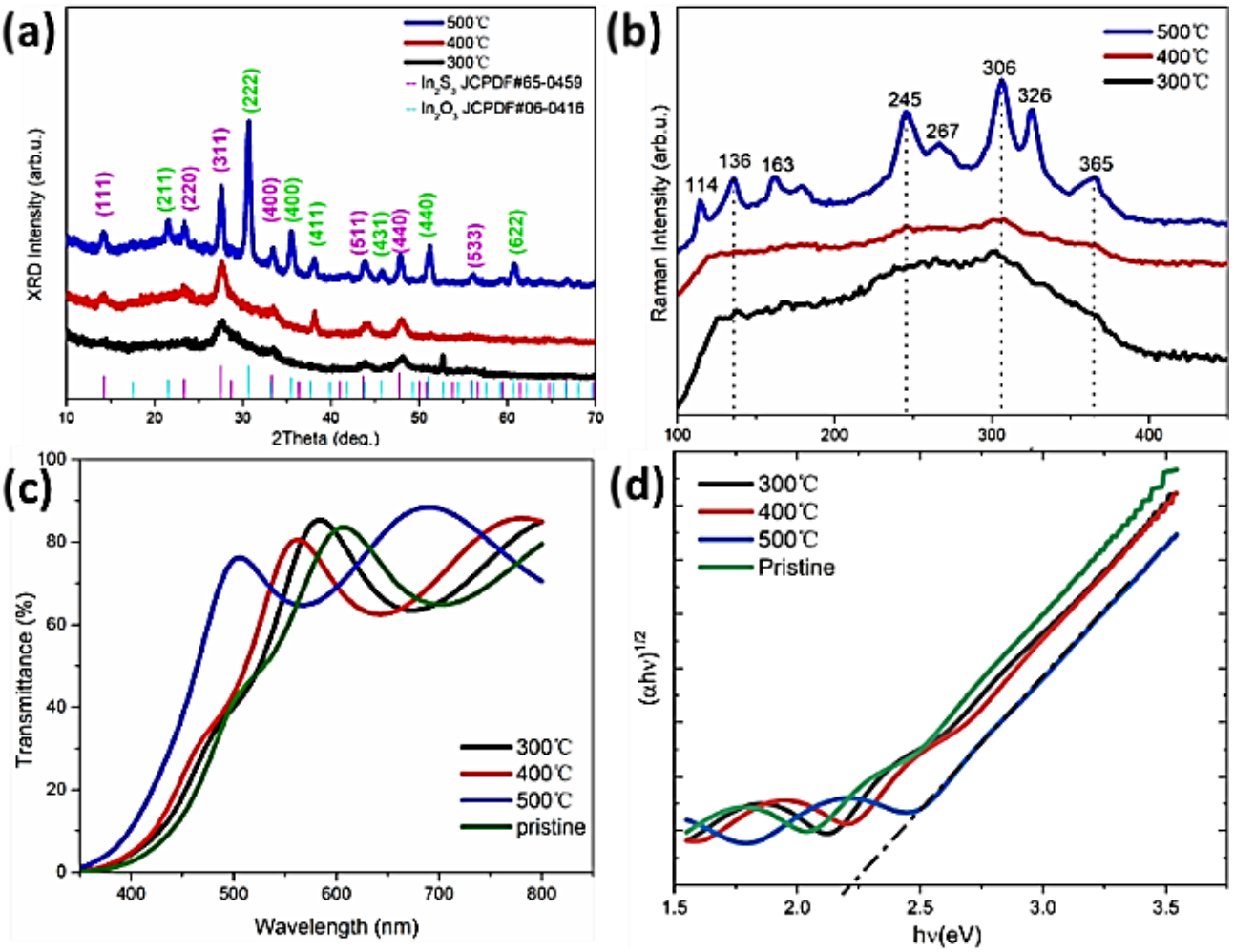

Fig. 2. (a) XRD pattern, (b) Raman spectra, (c) UV-Vis spectra and (d) the calculated optical bandgaps of the films annealed at different temperatures (color online)

Given the amorphous structure of the films prepared at different sputtering powers and growth times, subsequent annealing was conducted to the films. Fig. 2b shows the XRD pattern of the films annealed at different temperatures. It can be seen that the film begins to crystallize after annealing at 300 °C, and the diffraction peaks correspond to the crystal faces (111), (311), (400), (511), and (440) of cubic β-phase indium sulfide (JCPDF: 65-0459) [5]. As the annealing temperature increases to 400 °C, a new diffraction peak belonging to the crystal face (411) of indium oxide appears (JCPDF: 06-0416). Further higher temperature annealing at 500 °C, the diffraction peaks of indium sulfide become more obvious, which means better crystallization than lower annealing temperatures. However, more diffraction peaks belonging to the crystal faces (212), (222), (400), (431), (440), and (622) of indium oxide appear, which may be caused by unavoidable oxygen pollution during annealing [26]. By analyzing the corresponding Raman spectra (Fig. 2c), it can be seen that there are no obvious Raman peaks after annealing at 300 °C and 400 °C. But there are distinct Raman peaks belonging to α-indium sulfide (245, 267, 306, 326, and 365 cm^{-1}) and indium oxide (114, 136, 163 cm^{-1}) after annealing at 500 °C [24]. This confirms the XRD results that annealing at 500 °C results in the formation of indium oxide. The films' UV-Vis spectra also confirm the presence of indium oxide after annealing at high temperature (Fig. 2c) because of the apparent blue shift of the absorption band edge. The Tauc plot is used to determine the optical bandgap of the films[27]. The absorption coefficient (α) is deduced from the transmittance (T) by the formula $\alpha=-\ln T/d$ with the average film thickness (d) of 150 nm. By plotting $(\alpha h\nu)^{1/2}$ for indirect transition as a function of photon energy (hν), the optical band gap E_g is determined through extrapolating the linear portion to αhν=0. As shown in Fig. 2d, α obeys the indirect transition very well, indicating the prepared In_2S_3 films are indirect semiconductors[28]. The obtained optical band gaps are 1.98, 2.04, 2.08, and 2.20 eV, corresponding to the pristine, 300 °C, 400 °C, and 500 °C annealed films. The bandgap of indium oxide is from 2.70 eV to 3.72 eV according to the literatures[29, 30]. Therefore, the indium sulfide thin film with minor indium oxide will have large optical bandgap, and the formed In_2S_3/In_2O_3 heterostructure will facilitate the photoexcited electrons and holes separation effectively[26]. It is worth noting that the sub-band absorption is evident at about 500 nm for the films annealed at 300 °C and 400 °C,

which also indicates that the obtained films have the characteristics of multi-band absorptions [1, 31].

The film annealed at 500 °C has good crystallinity and light absorption properties, so electrical characterizations were further performed on this film. From the linear current-voltage curve of the indium sulfide film on the glass substrate of Fig. 3a, it can be concluded that the gold electrode has good ohmic contact with the indium sulfide film. Besides, the current-voltage curve between coplanar electrodes of indium sulfide film on the silicon substrate in Fig. 3b shows a standard back-to-back S shape, indicating a formed p-n junction between indium sulfide and the silicon substrate. The current-voltage curve of In_2S_3/Si heterostructure shown in Fig. 3c confirms the existence of Schottky contact. The solar cell conversion efficiency of the In_2S_3/Si heterostructure was measured, and the results are shown in Fig. 3d. It can be seen that the film exhibits certain photovoltaic conversion characteristics, but the efficiency is very low, which may be due to the indium sulfide films' poor crystalline, the low multi-band absorption efficiency, and the inappropriate metal contacts.

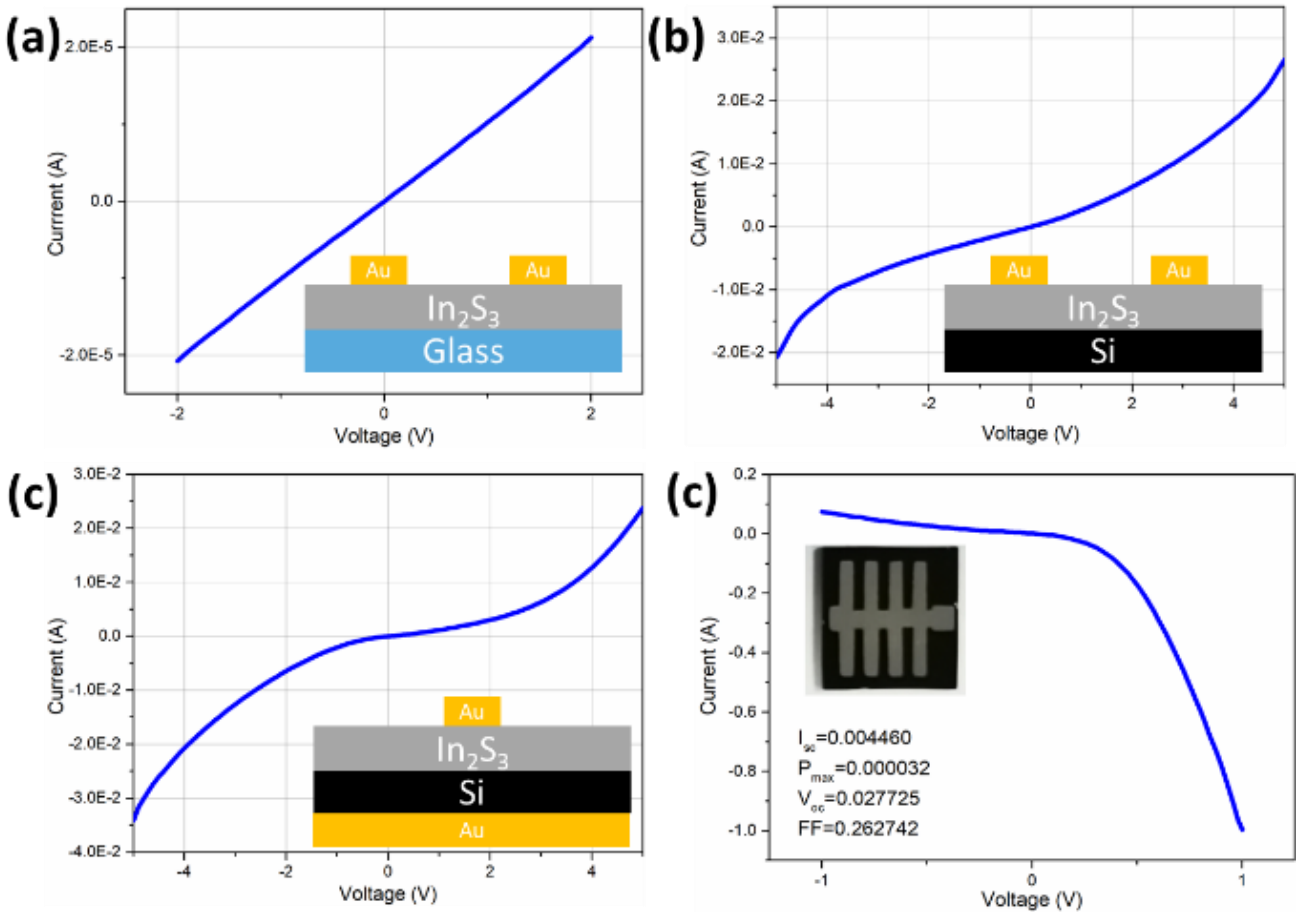

Fig. 3. Current-voltage curve of In_2S_3 thin film on (a) glass and (b) Si substrates between coplanar electrodes, the current-voltage curve of In_2S_3/Si heterostructure (c) in the dark and (d) under light illumination (color online)

4. Conclusions

Indium sulfide films have been prepared by magnetron sputtering, and their structural, optical, and electrical properties were characterized. The films prepared without intentional heating are amorphous. The subsequent annealing leads to the crystallization of indium sulfide. The film annealed at 500 °C presents apparent blue absorption band edge and multi-band absorptions, leading to a p-n junction between In_2S_3/Si heterostructure. The photovoltaic conversion is demonstrated, and more studies should be done in the future.

Acknowledgments

This work was supported by the Open Fund of Key Laboratory of Photovoltaic, Gansu Province, (No: 2017-1), the Science and Technology Program of Gansu Province (No: 18ZD2WA007), the Science and Technology Program of Gansu Natural Energy Research Institute (No: 2018YF-

04), and the Fundamental Research Funds for the Central Universities (Nos: lzujbky-2019-86, lzujbky-2020-kb06).

References

[1] Raquel Lucena, Irene Aguilera, Pablo Palacios, Perla Wahnón, José C. Conesa, Chem. Mater. **20**(16), 5125 (2008).
[2] Paul Pistor, Jose M Merino Álvarez, Máximo León, Marco Di Michiel, Susan Schorr, Reiner Klenk, Sebastian Lehmann, Acta. Crystallogr. B **72**(3), 410 (2016).
[3] Xianliang Fu, Xuxu Wang, Zhixin Chen, Zizhong Zhang, Zhaohui Li, Dennis Y. C. Leung, Ling Wu, Xianzhi Fu, Appl. Catal. B **95**(3), 393 (2010).
[4] Wenjuan Huang, Lin Gan, Haotian Yang, Nan Zhou, Renyan Wang, Wanhui Wu, Huiqiao Li, Ying Ma, Haibo Zeng, Tianyou Zhai, Adv. Funct. Mater. **27**(36), 1702448 (2017).
[5] SeongYeon Kim, Md Salahuddin Mina, Kiwhan Kim, Jihye Gwak, JunHo Kim, Sustain. Energ. Fuels **4**(1), 362 (2020).
[6] Bo Yang, Ming Wang, Xiaofei Hu, Tingwei Zhou, Zhigang Zang, Nano Energy **57**, 718 (2019).
[7] Ping Chen, Haijie Chen, Mingsheng Qin, Chongyin Yang, Wei Zhao, Yufeng Liu, Wenqing Zhang, Fuqiang Huang, J. Appl. Phys. **113**(21), 213509 (2013).
[8] Wei Tian, Cheng Chen, Linxing Meng, Weiwei Xu, Fengren Cao, Liang Li, Adv. Energy Mater. **10**(18), 1903951 (2020).
[9] Junying Liu, Sanjay Jatav, Eric H. Hill, Chem. Mater. **32**(23), 10015 (2020).
[10] Haijin Li, Yuying Gao, Yong Zhou, Fengtao Fan, Qiutong Han, Qinfeng Xu, Xiaoyong Wang, Min Xiao, Can Li, Zhigang Zou, Nano Lett. **16**(9), 5547 (2016).
[11] Jianting Lu, Jiahao Yan, Jiandong Yao, Zhaoqiang Zheng, Bijun Mao, Yu Zhao, Jingbo Li, Adv. Funct. Mater. **31**(8), 2007987 (2020).
[12] Sibo Wang, Bu Yuan Guan, Yan Lu, Xiong Wen David Lou, J. Am. Chem. Soc. **139**(48), 17305 (2017).
[13] Jungang Hou, Shuyan Cao, Yiqing Sun, Yunzhen Wu, Fei Liang, Zheshuai Lin, Licheng Sun, Adv. Energy Mater. **8**(9), 1701114 (2018).
[14] Linxing Meng, Min Wang, Haoxuan Sun, Wei Tian, Chenhong Xiao, Shaolong Wu, Fengren Cao, Liang Li, Adv. Mater. **32**(30), 2002893 (2020).
[15] A. Timoumi, H. Bouzouita, M. Kanzari, B. Rezig, Thin Solid Films **480**, 124 (2005).
[16] Maqsood Ali Mughal, Robert Engelken, M. Jason Newell, Joshua Vangilder, Shyam Thapa, Kayla Wood, B. Ross Carroll, J. Bruce Johnson, J. Electrochem. Soc. **162**(7), D265 (2015).
[17] Shaibal K. Sarkar, Jin Young Kim, David N. Goldstein, Nathan R. Neale, Kai Zhu, C. Michael Elliott, Arthur J. Frank, Steven M. George, J. Phys. Chem. C **114**(17), 8032 (2010).
[18] Wha Tek Kim, Chang Dae Kim, J. Appl. Phys. **60**(7), 2631 (1986).
[19] Sebastian Siol, Tara P. Dhakal, Ganesh S. Gudavalli, Pravakar P. Rajbhandari, Clay DeHart, Lauryn L. Baranowski, Andriy Zakutayev, ACS Appl. Mater. Interfaces **8**(22), 14004 (2016).
[20] Sreejith Karthikeyan, Arthur E. Hill, Richard D. Pilkington, Appl. Surf. Sci. **418**, 199 (2017).
[21] Yaxin Ji, Yufeng Ou, Zhou Yu, Yong Yan, Dan Wang, Chuanpeng Yan, Lian Liu, Yong Zhang, Yong Zhao, Surface and Coatings Technology **276**, 587 (2015).
[22] Dong Hyun Hwang, Shinho Cho, Kwun Nam Hui, Young Guk Son, J. Nanosci. Nanotechnol. **14**(12), 8978 (2014).
[23] Zhenxing Zhang, Jian Li, Haijun Zhang, Xiaojun Pan, Erqing Xie, J. Alloys. Compd. **549**, 88 (2013).
[24] H. Izadneshana, V. F. Gremenok, Journal of Applied Spectroscopy **81**(5), 765 (2014).
[25] Han-Yong Joo, Hyeong Joon Kim, Sang June Kim, Sang Youl Kim, J. Vac. Sci. Technol. A **17**(3), 862 (1999).
[26] Huichang Xu, Yu Wang, Xiaoli Dong, Nan Zheng, Hongchao Ma, Xiufang Zhang, Appl. Catal. B **257**, 117932 (2019).
[27] Z. X. Zhang, X. J. Pan, L. X. Liu, Z. W. Ma, H. T. Zhao, L. Jia, E. Q. Xie, J. Appl. Phys. **105**(1), 016101 (2009).
[28] N. Barreau, A. Mokrani, F. Couzinié-Devy, J. Kessler, Thin Solid Films **517**(7), 2316 (2009).
[29] Roland Marschall, Adv. Funct. Mater. **24**(17), 2421 (2014).
[30] Soumitra Kar, Supriya Chakrabarti, Subhadra Chaudhuri, Nanotechnology **17**(12), 3058 (2006).
[31] Perla Wahnón, José C. Conesa, Pablo Palacios, Raquel Lucena, Irene Aguilera, Yohanna Seminovski, Fernando Fresno, Phys. Chem. Chem. Phys. **13**(45), 20401 (2011).

* Corresponding authors. qiao@gneri.com.cn; zhangzx@lzu.edu.cn